Exceptional Activity for Methane Combustion over Modular Pd@CeO_2 Subunits on Functionalized Al_2O_3

M. Cargnello,[1] J. J. Delgado Jaén,[2] J. C. Hernández Garrido,[2] K. Bakhmutsky,[3] T. Montini,[1] J. J. Calvino Gámez,[2] R. J. Gorte,[3]* P. Fornasiero[1]*

There is a critical need for improved methane-oxidation catalysts to both reduce emissions of methane, a greenhouse gas, and improve the performance of gas turbines. However, materials that are currently available either have low activity below 400°C or are unstable at higher temperatures. Here, we describe a supramolecular approach in which single units composed of a palladium (Pd) core and a ceria (CeO_2) shell are preorganized in solution and then homogeneously deposited onto a modified hydrophobic alumina. Electron microscopy and other structural methods revealed that the Pd cores remained isolated even after heating the catalyst to 850°C. Enhanced metal-support interactions led to exceptionally high methane oxidation, with complete conversion below 400°C and outstanding thermal stability under demanding conditions.

Methane (CH_4) is the largest constituent of natural gas and is widely used in power generation and in other heating applications. However, the release of unburned CH_4 during homogeneous combustion is a serious problem, given that CH_4 is a greenhouse gas with an effect that is 20 times higher than that of CO_2. Presently available, emissions-control catalysts are notoriously ineffective at reducing concentrations of CH_4 in exhaust streams. High-temperature combustion also results in the emission of toxic nitrogen oxides (NO_x) and CO. Combustion of CH_4 promoted by heterogeneous catalysts could utilize the available energy of methane at lower temperatures, increasing system performance and limiting emissions by drastically reducing the required temperatures (*1*).

Given the high stability of CH_4, heterogeneous catalysts for methane oxidation must be very active at low reaction temperatures (below at least 400°C). Furthermore, materials for this application must also be catalytically and mechanically stable at high reaction and flame temperatures (*2*). PdO_x supported on alumina or zirconia is recognized as one of the best catalysts for catalytic CH_4 oxidation (*3*), even if the active phase of the catalysts is still disputed. Unfortunately, Pd-based catalysts tend to deactivate through loss of active surface by sintering and by transformation into metallic Pd at temperatures above 600°C (*4*). Both experimental and theoretical studies reveal that ceria (CeO_2) can improve the catalytic activity of supported Pd by stabilizing PdO_x (*5*–*8*), but pure CeO_2 has limited thermal stability. Other systems based on metal oxides have been studied, but their activity is generally much lower, with complete CH_4 conversion obtained only above 600°C (*2*). Materials that could simultaneously enhance the performance of Pd-based catalysts at low temperatures and limit deactivation at elevated temperatures would greatly improve catalytic CH_4 combustion processes.

The tailored positioning of the building blocks at the nanometer scale can markedly improve the performance of the materials through electronic and steric interactions. Heterogeneous catalysts that are used in a wide variety of industrial and environmental applications already take advantage of the synergy between a support and the supported phases. Some oxides, such as ceria, can participate in the catalytic cycle by providing reactive oxygen through formation of vacancies (*9*, *10*). In this case, it is essential that the catalytic sites be located in close proximity to the interface area between the metal particles and the oxide support. Indeed, dual-site mechanisms, where reactants are activated at the metal-support interface, are known to exist (*11*).

Core-shell structures are special cases in which metal-support interactions are enhanced by maximizing this interface (*12*). The strong interactions between the components of the core and the shell can lead to advanced materials for catalytic (*13*, *14*) and photocatalytic (*15*) applications. Besides the possibility of improved catalytic performance, the self-assembly, core-shell approach offers a powerful tool for minimizing deactivation of the catalyst by metal sintering processes (*12*, *16*). These phenomena are particularly pronounced for high-temperature reactions, as is the case of CH_4 combustion (*7*).

Here, we report on a hierarchical design of core-shell type catalysts inspired by the concepts of supramolecular chemistry (*17*) in which the building blocks are preorganized in a way to exploit their catalytic interactions to the maximum extent. Supramolecular chemistry concepts have not been widely applied in heterogeneous catalysis because of the difficulty in manipulating the metal-support interaction at the nanoscale. Two active building blocks, Pd and CeO_2, were prepared separately, then self-assembled and organized in solution to form supramolecular core-shell structures held together by metal ion–ligand coordination interactions. We exploited the preorganization of the functionalized Pd@CeO_2 core-shell structures to disperse single units onto a modified, catalytically inert alumina carrier. Transmission electron microscopy (TEM) revealed that single isolated structures were deposited and maintained even after severe thermal treatments at temperatures up to 850°C. The special configuration of the hierarchical catalyst led to exceptionally high and stable performance for the catalytic combustion of methane with reduced amounts of Pd and ceria. This particular geometry appears to stabilize the active phase of the catalyst, suppressing agglomeration of the metal particles upon high-temperature calcination and increasing the concentration of PdO_x.

The supramolecular Pd@CeO_2 core-shell structures were prepared according to our recently published procedure (*18*). This method is based on the self-assembly between functionalized metallic Pd particles (~2 nm) protected by 11-mercaptoundecanoic acid (MUA) and a Ce(IV) alkoxide. It takes advantage of a strategic combination of interactions; the first of these occurs between the thiol group of MUA and Pd, and the second one is between the carboxyl group of the MUA and Ce(IV) moieties. A controlled hydrolysis in the presence of dodecanoic acid of the resulting assembled units leads to the formation of the Pd@CeO_2 structures, in which the CeO_2 shell is composed of small crystallites (~3 nm) organized around the preformed Pd particles. The structures are dispersible in common low-polarity solvents such as tetrahydrofuran, dichloromethane, toluene, and other hydrocarbons and are amenable for controlled deposition onto different substrates. Furthermore, the extension of this procedure to other core-shell compositions [Pd and Pt as core; TiO_2, ZrO_2, and CeO_2 as shells (*19*)] gives to the present approach a wide applicability and versatility.

We previously demonstrated that the Pd@CeO_2 structures can be deposited onto pristine, commercial alumina, resulting in redox properties and catalytic performances different from those of conventional or bulk materials (*20*). However, because pristine alumina is highly hydrophilic (*21*), we observed minimal interactions between the alumina support and the hydrophobic Pd@CeO_2 structures, so that the Pd@CeO_2 structures tended to agglomerate with one another rather than adhering to the support (Fig. 1A). This agglomeration was confirmed by high-angle annular dark field (HAADF)–scanning transmission electron microscopy (STEM) images collected at different tilting angles [figs. S1 and S2 (*22*)]. The active-phase agglomeration may introduce the generation of hot spots and deactivate the catalyst by sintering, so it was crucial to develop a synthetic

[1]Department of Chemical and Pharmaceutical Sciences, ICCOM-CNR, Consortium INSTM, University of Trieste, via L. Giorgieri 1, 34127 Trieste, Italy. [2]Departamento de Ciencia de los Materiales e Ingeniería Metalúrgica y Química Inorgánica, Facultad de Ciencias, Universidad de Cádiz, Campus Río San Pedro, 11510 Puerto Real, Cádiz, Spain. [3]Department of Chemical and Biomolecular Engineering, University of Pennsylvania, 311A Towne Building, 220 South 33rd Street, Philadelphia, PA 19104, USA.

*To whom correspondence should be addressed. E-mail: gorte@seas.upenn.edu (R.J.G.); pfornasiero@units.it (P.F.)

strategy able to deposit the Pd@CeO_2 as single units on the support.

The alumina surface was first made hydrophobic by reacting it with an organosilane, triethoxy(octyl)silane (TEOOS) (Fig. 1B) (*23*). Because this silane has three alkoxy groups that are prone to hydrolysis and one alkyl chain that is not, the reaction between the silane and alumina can lead to one of the following two situations (*24*): Either the silanol groups formed by hydrolysis of the ethoxy ligands can react with OH groups of the alumina surface to form oxane bonds of the type Si-O-Al, or the silane molecules can react with each other to give multimolecular structures of bound silanes on the surface. In both cases, the strong Si-C bond ensures that the hydrophobic chain is attached to Si moieties, causing the surface of alumina to be covered by alkyl chains. In addition, the presence of Si can also benefit the reducibility of the supported CeO_2 (*25*). A movie of water droplets (colored by means of $FeCl_3$ for clarity) poured on a powdery layer of both pristine and hydrophobic alumina demonstrates the efficiency of the adopted strategy [movie S1 (*22*)]. The water droplets deposited on the pristine alumina immediately spread on the powder as a consequence of the favorable interactions with the alumina OH groups. By contrast, the water droplets deposited on the hydrophobic alumina were repulsed. Fourier-transform infrared analysis confirmed the formation of alkyl chain attachments onto the surface of alumina [fig. S3 (*22*)].

Hydrophobic Al_2O_3 (hereafter referred to as H-Al_2O_3) exhibited much greater capacity for the adsorption of the Pd@CeO_2 structures compared to the pristine, hydrophilic Al_2O_3. The adsorption resulted in a color change of the supernatant solution [fig. S4 (*22*)], which was almost colorless when adsorbed onto hydrophobic alumina but dark when adsorbed onto pristine alumina. To quantitatively measure the adsorption of Pd@CeO_2 structures on H-Al_2O_3, we measured the absorbance at 500 nm for a solution of Pd@CeO_2 after the addition of varying amounts of H-Al_2O_3. Because the solution of Pd@CeO_2 structures shows a broad absorption band in the ultraviolet-visible region (the Pd to CeO_2 weight ratio was fixed at 1:9) [inset of fig. S5 (*22*)], the concentration of Pd@CeO_2 structures remaining in solution can be inferred from the intensity of the absorption. The absorbance of the supernatant versus loading curve showed a characteristic sigmoidal shape, with a sharp increase for attempted loadings greater than 1 weight % (wt %), indicating that the H-Al_2O_3 surface became saturated at coverages higher than this. Notably, this loading is approximately half of that expected for a theoretical monolayer, assuming the Pd@CeO_2 structures pack in a close-packed configuration over the entire available surface area {likely because only one-half of the surface area of the H-Al_2O_3 is associated with mesopores that have a diameter smaller than that of the Pd@CeO_2 units, ~15 nm in dimension as prepared, preventing these pores from contributing to the adsorption process [fig. S6 (*22*)]}. The deposition of Pd@CeO_2 onto H-Al_2O_3 also led to the formation of pores with diameters smaller than 10 nm that were not present in the original H-Al_2O_3 [inset of fig. S6, part B (*22*)]. These pores could be associated with the Pd@CeO_2 units themselves (*18*). The porous nature of the CeO_2 shell is indeed corroborated by CO chemisorption data (see below), which demonstrates the accessibility of Pd. The requirement of having the proper support pore sizes for deposition of Pd@CeO_2 onto the alumina was further demonstrated by our attempts to deposit these structures onto hydrophobic Fe_2O_3 and SiO_2 samples, materials with narrow pore-size distributions but smaller pore size than Al_2O_3 [fig. S7 (*22*)]. With both hydrophobic Fe_2O_3 that had an average pore diameter of 13 nm and SiO_2 that had an average pore diameter of 4 nm, very little adsorption of the Pd@CeO_2 structures was observed, despite the very high surface area in the SiO_2 support.

Several electron microscopy techniques were used to demonstrate that single Pd@CeO_2 supramolecular structures were successfully deposited onto the hydrophobic alumina (Fig. 2). HAADF-STEM images (Fig. 2, A, B, and D) show Pd@CeO_2 as small bright spots on the underlying surface of the hydrophobic alumina crystallites. The Pd@CeO_2 units are well dispersed and well separated throughout the entire supporting material. Images collected at different tilting angles confirmed that the structures were indeed single units [fig. S1 (*22*)]. X-ray energy dispersive spectroscopy (EDS) analysis with a very fine probe (0.5 nm) confirmed that the bright spots are composed of Pd and Ce with the correct, initial weight ratio (Fig. 2C). By analyzing more than 50 single spots, we found both Pd and Ce to be associated in 49 of 50 spot analyses, thus demonstrating that the core-shell structures are intact and do not segregate after the deposition and calcination to 850°C. One spot showed the presence of only CeO_2 (spot 3 of Fig. 2C); a small concentration of CeO_2 nanoparticles may have been produced in the initial synthesis, or excess ceria on the Pd@CeO_2 particles may have been removed during the calcination of the supported catalyst to 850°C. After the calcination at 500°C, EDS line profiles clearly revealed single Pd@CeO_2 structures, showing that the Pd signal arose from the core (Fig. 2E); high-resolution electron microscopy (Fig. 2F) further confirmed a core-shell structure. White boxes in Fig. 2F highlight a single Pd@CeO_2 particle, and selected digital diffraction patterns demonstrate the presence of Pd in the core and of ceria in the outer layer. CeO_2 crystallites were ~3 nm in size, in agreement with line broadening of the powder x-ray diffraction lines (fig. S8). These small Pd crystallites were maintained even after calcination at 850°C, and this stabilization was almost certainly

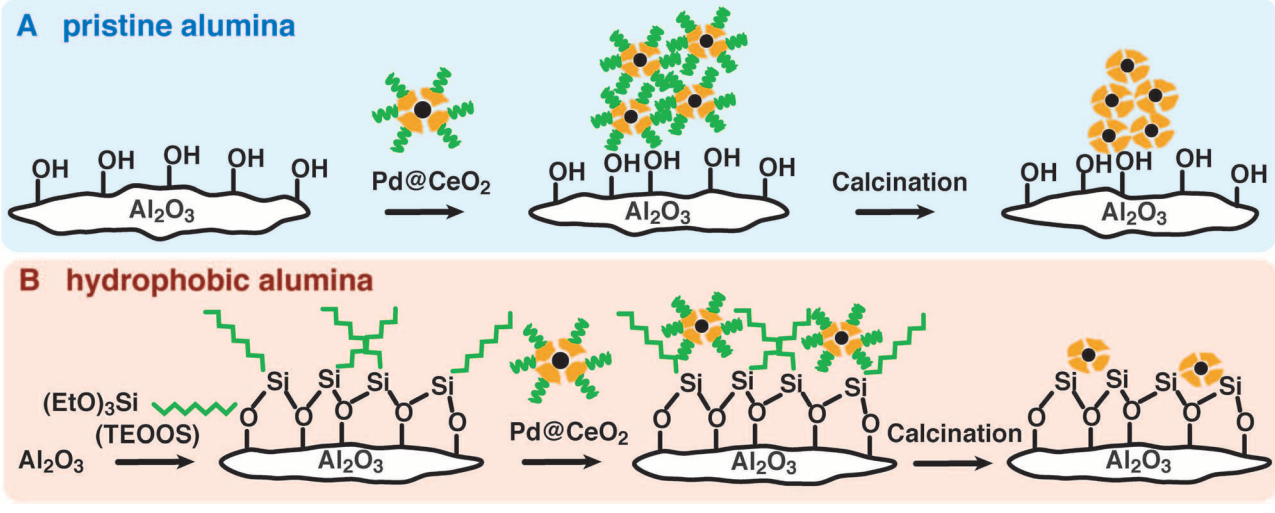

Fig. 1. Schematic representation of the agglomeration of Pd@CeO_2 structures when using the pristine alumina (**A**) and their deposition as single units after treatment of the same support with triethoxy(octyl)silane (TEOOS) (**B**).

a result of the core-shell configuration, where the organization of the crystallites around the preformed Pd particles avoids their agglomeration. In any case, Pd was always associated with a surrounding CeO_2 layer, so that there was no indication that the Pd@CeO_2 particles had decomposed. Furthermore, although the CeO_2 shell is porous, the results suggest that intimate contact between the components can reduce the occurrence of Ostwald ripening (see also below).

A model of the Pd@CeO_2 units that are present on our support is shown in movie S2. The structure, which is formed by a central Pd nanoparticle (about 1.8 nm in diameter) surrounded by 11 CeO_2 nanocrystals, has the expected final weight ratios (1 and 9%, respectively). In some orientations, the Pd nanoparticle is completely hidden by the surrounding ceria nanocrystals, demonstrating the difficulty of imaging these structures by microscopy. The microscopy data provide conclusive evidence that the core-shell structure of the single Pd@CeO_2 units remains intact and show that these structures possess a high thermal stability upon deposition on the hydrophobic alumina.

The Pd@CeO_2/H-Al_2O_3 catalysts were tested for the combustion of CH_4 ($CH_4 + 2O_2 \rightarrow CO_2 + 2H_2O$). To compare the effect of the nanostructure on the catalytic activity, we prepared additional reference samples using conventional synthetic procedures. The first reference catalyst consisted of 1 wt % Pd on a CeO_2 support, prepared by optimized incipient wetness impregnation (denoted as Pd/CeO_2-IWI). A second reference sample was prepared by impregnation of Pd (at 1 wt %) and CeO_2 (at 9 wt %) from their nitrate salts onto pristine alumina (denoted as Pd/CeO_2/Al_2O_3-IMP). These and two additional reference samples are described in the supplementary materials (fig. S9). All of the catalysts were calcined at 850°C for 5 hours and tested under the same reaction conditions.

CO chemisorption experiments confirmed the accessibility of the Pd phase in all the catalysts (table S1). The thermal stability of the Pd@CeO_2/H-Al_2O_3 catalyst against sintering was confirmed by the average Pd particle size after calcination at 850°C (2.2 nm) being very close to that of the initial starting Pd nanoparticles. The Pd/CeO_2/Al_2O_3-IMP sample demonstrated poor thermal stability and had an average Pd particle size of 6.0 nm after calcination. The Pd/CeO_2-IWI sample exhibited a small average particle size (1.9 nm), in accordance with previous reports for materials obtained by using similar preparation methods (*7*, *26*). The Pd@CeO_2/H-Al_2O_3 catalysts prepared with different loadings of the structures (Pd/Ce weight ratio was kept at 1/9) showed similar metal dispersions as measured by CO chemisorption (table S1), in accordance with the molecular nature of the Pd@CeO_2 units.

The Pd@CeO_2/H-Al_2O_3 material demonstrated outstanding catalytic performance. Complete conversion of CH_4 was observed for a gas stream of 0.5 volume % CH_4 and 2.0 volume % O_2 in Ar at a space velocity of 200,000 ml g^{-1} $hour^{-1}$ at about 400°C (Fig. 3). By comparison, all the other reference samples achieved complete CH_4 conversion only above 700°C (fig. S9), more than 300° higher than that found with the Pd@CeO_2/H-Al_2O_3 catalyst. Even when compared to state-of-the-art Pd/CeO_2 systems under the same reaction conditions, the temperature of complete conversion is decreased by more than 130°C (*7*). The enhanced reactivity of the Pd@CeO_2/H-Al_2O_3 catalyst is almost certainly the result of the strong Pd-CeO_2 interaction of the core-shell Pd@CeO_2 units. These interactions are not as optimal in the Pd/CeO_2-IWI catalyst, whereas some Pd may not even be in contact with CeO_2 in the Pd/CeO_2/Al_2O_3-IMP sample, resulting in lower activities when compared to the Pd@CeO_2/H-Al_2O_3 catalyst.

PdO_x is commonly recognized as the active phase for this reaction (*1*). In the 650° to 850°C temperature range, PdO decomposes to the thermodynamically stable Pd metal, which is much less active (*1*, *3*). The formation of metallic Pd decreases the rates for CH_4 combustion and is commonly observed as a transient decrease in the CH_4 conversion in light-off curves for both supported and unsupported Pd-based systems (*3*). The nature of the support can modify this behavior, and the presence of CeO_2 can shift the temperature window in which this transition occurs, provided that there is good contact between Pd and ceria (*6*). Pd@CeO_2/H-Al_2O_3 showed a stable activity for CH_4 oxidation over the entire range of temperatures studied (250° to 850°C) (Fig. 3A), with no decrease in activity during either heating or cooling curves. By contrast, the reference samples clearly show the usual transient decrease in CH_4 conversion, both during the

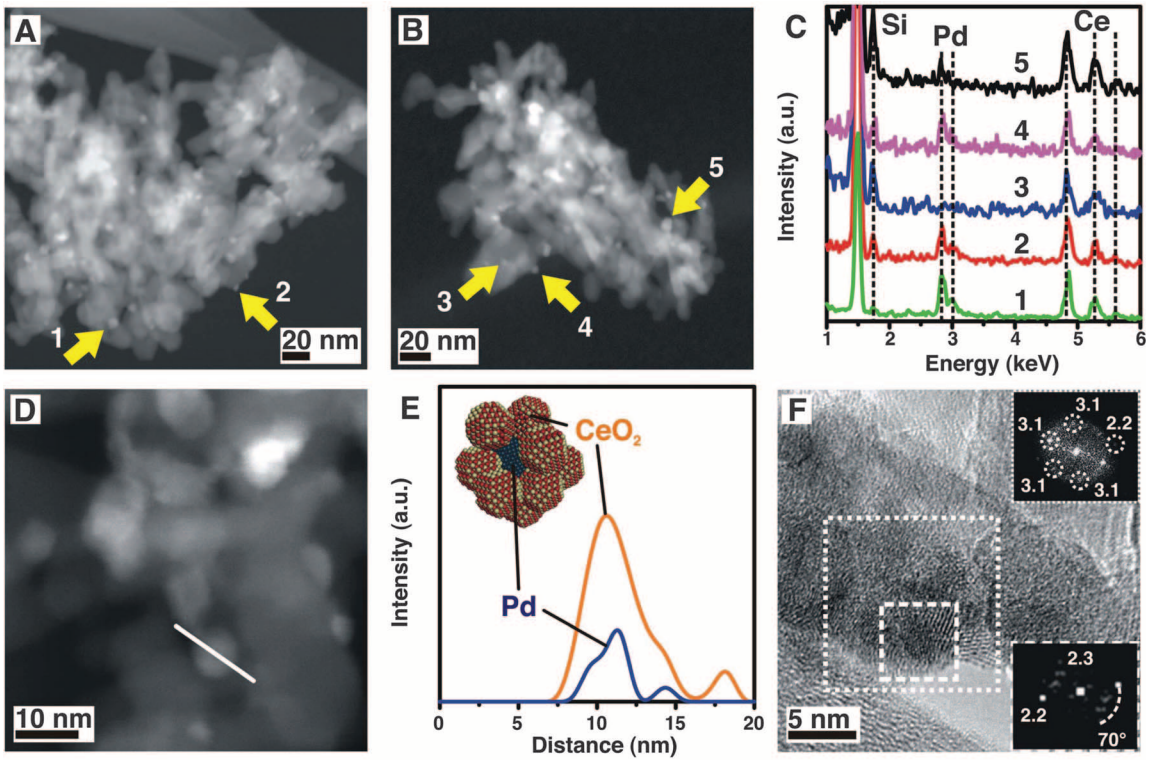

Fig. 2. TEM investigations of Pd@CeO_2 core-shell structures dispersed on hydrophobic alumina. (**A**) HAADF-STEM image after calcining to 500°C for 5 hours and (**B**) to 850°C for 5 hours. (**C**) EDS spot analysis of the indicated particles. (**D**) High-magnification HAADF-STEM image of the Pd@CeO_2/H-Al_2O_3 catalysts calcined to 500°C and (**E**) the corresponding EDS line profile together with a model [see also supplementary materials and movie S2]. (**F**) HRTEM image of a single Pd@CeO_2 structure on the Pd@CeO_2/H-Al_2O_3 catalysts calcined to 500°C. The digital diffraction patterns of the particles in the white squares are reported in the top-right and bottom-right insets together with representative bond distances (Å) and bond angles for Pd and ceria.

heating and the cooling portions of the curves at temperatures between 600° and 750°C, in agreement with previous reports (*4*). To our knowledge, such strong inhibition of the dip deactivation in the conversion curve in Pd-based catalysts for catalytic CH_4 oxidation has not been observed previously, a result that again points to a special role of the CeO_2 in the core-shell configuration in stabilizing the active phase of the catalyst. The maximized metal-support interface area and the well-known oxygen donation capability of CeO_2 can favor the oxidation of Pd nanoparticles, sustaining the catalytic reaction in the entire range of investigated temperatures.

To gain further insights, we conducted temperature-programmed oxidation experiments on the three samples (fig. S10). A PdO-Pd transition is observed in each of the samples, but is shifted to higher temperatures on the Pd@CeO_2/H-Al_2O_3 sample. Also, there is a direct relationship between the amount of oxygen released in the upward temperature ramp and taken up in the cooling ramp and the sample activity. This indicates that transformation of metallic Pd into PdO_x is maximized in the supramolecular catalyst due to the close contact of ceria with Pd, explaining the much improved activity of Pd@CeO_2/H-Al_2O_3. Indeed, there was only a very small decrease in activity for the Pd@CeO_2/H-Al_2O_3 sample during cooling, even under extremely demanding reaction conditions (gas hourly space velocity of ~1,000,000 ml g^{-1} $hour^{-1}$) (fig. S11). Furthermore, the Pd@CeO_2/H-Al_2O_3 was stable to aging treatments at 850°C for 12 hours (fig. S12) and after subsequent run-up and cool-down experiments (fig. S13). CO chemisorption results on the Pd@CeO_2/H-Al_2O_3 sample, performed after catalytic tests (table S1), showed minimal evidence for Pd sintering and no evidence for redispersion of PdO, ruling out the contribution of this effect to the observed high, stable activity.

There are a number of possible explanations for why the ceria shell has such a pronounced effect in maintaining an oxidized Pd core. First, the thin ceria shell could well be under mechanical stress due to spatial confinement of individual Pd@CeO_2 units. It has recently been demonstrated that stress can positively affect the oxygen mobility (*27*). Second, the small CeO_2 crystallite size that is maintained as a result of the templating effect of the Pd cores likely leads to a high degree of disorder within the ceria shell, breaking the typical fluorite structure that stabilizes Ce^{4+} and thereby increasing the reducibility of the ceria shell (*28*). Third, the decoration of the Pd by ceria is not complete, because there is still appreciable adsorption of CO. This could lead to the formation of a high concentration of undercoordinated, reactive Pd sites at the interface between the metal and the oxide that are known to be more effective in CH_4 activation (*29*).

Kinetic rate data further corroborate the very high intrinsic activity of the supramolecular catalyst when compared to the reference catalysts (Fig. 4). The reaction rates on the Pd@CeO_2/H-Al_2O_3 sample were about 40 times higher than those on Pd/CeO_2-IWI and 200 times higher than on Pd/CeO_2/Al_2O_3-IMP, respectively, under the same experimental conditions (Fig. 4A). Furthermore, the rates were more than one order of magnitude higher than that of other optimized Pd-based catalysts (*7*). CO adsorption data (table S1) demonstrated that the difference in activity cannot be related to the amount of exposed Pd because the Pd/CeO_2-IWI sample showed a higher Pd accessibility than that of the Pd@CeO_2/H-Al_2O_3 core-shell catalyst (60% versus 50%, respectively). The apparent activation energies for each of the catalysts were also similar (90 to 120 kJ mol^{-1}) and slightly lower than those in the literature (*7*), but implying that the nature of the active sites in Pd@CeO_2/H-Al_2O_3 are similar to that of the other two catalysts. Notably, the number of active sites was markedly increased in the Pd@CeO_2/H-Al_2O_3 sample by means of the special configuration, as evidenced by the larger preexponential factor and turn-over-frequency values (table S2). Furthermore, samples prepared at different Pd loadings (Pd/Ce weight ratio was maintained at 1/9) showed very similar reaction rates when normalized by the amount of metal (Fig. 4B) and exhibited identical activation energies (100 to 110 kJ mol^{-1}).

The data presented here demonstrate that the Pd@CeO_2 structures deposited as single units on the hydrophobic alumina act as supramolecular catalysts. In these structures, the synergy between Pd and CeO_2 produces active sites that are equally active in all of the samples, though in different

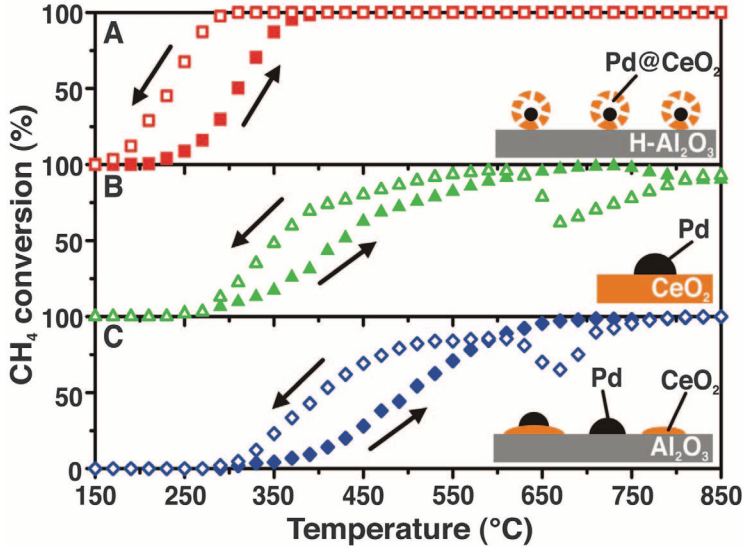

Fig. 3. Heating and cooling (10°C min^{-1}) light-off curves of CH_4 conversion against the temperature for the three catalyst formulations used. (**A**) Pd@CeO_2/H-Al_2O_3 core-shell catalyst, (**B**) Pd/CeO_2-IWI, and (**C**) Pd/CeO_2/Al_2O_3-IMP.

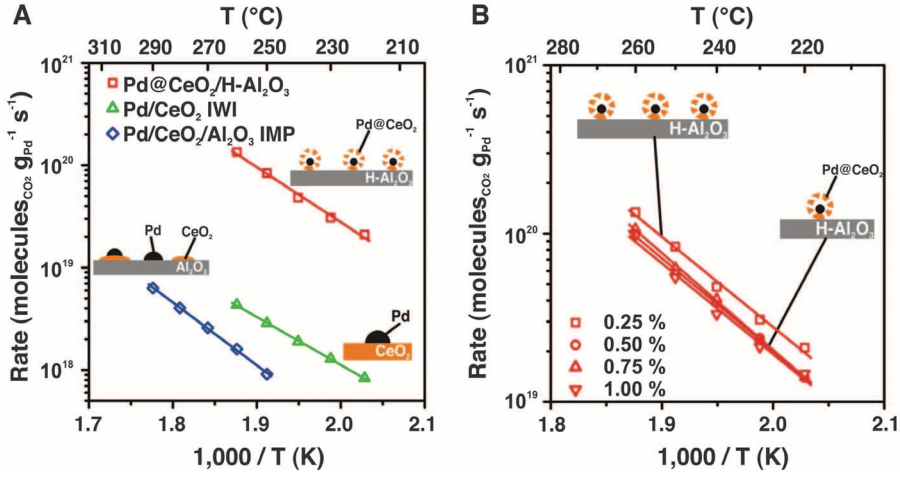

Fig. 4. Kinetic rate data for CH_4 oxidation on (**A**) Pd@CeO_2/H-Al_2O_3 core-shell catalyst, Pd/CeO_2-IWI, and Pd/CeO_2/Al_2O_3-IMP; (**B**) Pd@CeO_2/H-Al_2O_3 core-shell catalysts at different loadings of the structures (Pd/Ce weight ratio was kept at 1/9): Pd loading of 0.25, 0.50, 0.75, and 1.00%.

numbers. As a further confirmation, CO chemisorption results demonstrated very similar Pd accessibility for all of the Pd@CeO_2 samples prepared (table S2), corroborating the defined geometry and morphology obtained through the supramolecular approach. This approach could potentially be valuable even for three-way catalysts, where the special properties shown here could be important for improving the activity at low oxygen concentrations, enhancing stability against sintering, and protecting against poisoning through the core-shell configuration.

References and Notes

1. P. Gélin, M. Primet, *Appl. Catal. B* **39**, 1 (2002).
2. A. J. Zarur, J. Y. Ying, *Nature* **403**, 65 (2000).
3. P. Forzatti, *Catal. Today* **83**, 3 (2003).
4. R. J. Farrauto, M. C. Hobson, T. Kennelly, E. M. Waterman, *Appl. Catal. A* **81**, 227 (1992).
5. L. H. Xiao, K. P. Sun, X. L. Xu, X. N. Li, *Catal. Commun.* **6**, 796 (2005).
6. S. Colussi, A. Trovarelli, G. Groppi, J. Llorca, *Catal. Commun.* **8**, 1263 (2007).
7. S. Colussi *et al.*, *Angew. Chem. Int. Ed.* **48**, 8481 (2009).
8. A. D. Mayernick, M. J. Janik, *J. Catal.* **278**, 16 (2011).
9. A. Trovarelli, *Catal. Rev. Sci. Eng.* **38**, 439 (1996).
10. F. Esch *et al.*, *Science* **309**, 752 (2005).
11. I. X. Green, W. Tang, M. Neurock, J. T. Yates Jr., *Science* **333**, 736 (2011).
12. L. De Rogatis *et al.*, *ChemSusChem* **3**, 24 (2010).
13. C. M. Y. Yeung *et al.*, *J. Am. Chem. Soc.* **127**, 18010 (2005).
14. K. Tedsree *et al.*, *Nat. Nanotechnol.* **6**, 302 (2011).
15. V. Gombac *et al.*, *J. Phys. Chem. A* **114**, 3916 (2010).
16. J. Lu *et al.*, *Science* **335**, 1205 (2012).
17. J. M. Lehn, *Science* **260**, 1762 (1993).
18. M. Cargnello, N. L. Wieder, T. Montini, R. J. Gorte, P. Fornasiero, *J. Am. Chem. Soc.* **132**, 1402 (2010).
19. K. Bakhmutsky *et al.*, *ChemSusChem* **5**, 140 (2012).
20. N. L. Wieder *et al.*, *J. Phys. Chem. C* **115**, 915 (2011).
21. A. A. Tsyganenko, P. P. Mardilovich, *J. Chem. Soc., Faraday Trans.* **92**, 4843 (1996).
22. Materials, methods, and supporting data are available as supplementary materials on *Science* Online.
23. B. Paul, W. N. Martens, R. L. Frost, *J. Colloid Interface Sci.* **360**, 132 (2011).
24. A. A. Parker, *J. Adhes. Sci. Technol.* **16**, 679 (2002).
25. E. Rocchini *et al.*, *J. Catal.* **211**, 407 (2002).
26. S. Hinokuma, H. Fujii, M. Okamoto, K. Ikeue, M. Machida, *Chem. Mater.* **22**, 6183 (2010).
27. T. X. T. Sayle *et al.*, *Chem. Mater.* **24**, 1811 (2012).
28. G. Zhou, P. R. Shah, T. Montini, P. Fornasiero, R. J. Gorte, *Surf. Sci.* **601**, 2512 (2007).
29. J. Wei, E. Iglesia, *J. Phys. Chem. B* **108**, 4094 (2004).

Acknowledgments: M. Graziani (University of Trieste) is acknowledged for discussions. M.C., T.M., and P.F. acknowledge financial support from the University of Trieste through FRA 2011 project and Consorzio Interuniversitario Nazionale per la Scienza e Tecnologia dei Materiali (INSTM). R.J.G. and K.B. acknowledge support from the Air Force Office of Scientific Research (Multidisciplinary University Research Initiative) grant FA9550-08-1-0309. J.J.D.J., J.C.H.G., and J.J.C.G. acknowledge financial support through research project CSD2009-00013 from the Ministry of Science and Innovation of Spain. The Electron Microscopy Division of SCCyT at University of Cádiz is acknowledged. Author contributions: M.C., R.J.G., and P.F. conceived the idea for the study. M.C. synthesized the materials. J.J.D.J. performed TEM and STEM investigations, J.C.H.G. performed tomography investigations, and J.J.C.G coordinated the TEM characterization. M.C. performed catalytic tests and characterization of the materials. K.B. and T.M. contributed to the characterization and catalytic testing. M.C., R.J.G., and P.F. wrote the manuscript. All the authors commented on the data and the manuscript.

Supplementary Materials

www.sciencemag.org/cgi/content/full/337/6095/713/DC1
Materials and Methods
Figs. S1 to S13
Tables S1 and S2
Movies S1 and S2
References (*30*–*33*)

4 April 2012; accepted 28 June 2012
10.1126/science.1222887

Synthesis and Structure of a Terminal Uranium Nitride Complex

David M. King,[1] Floriana Tuna,[2] Eric J. L. McInnes,[2] Jonathan McMaster,[1] William Lewis,[1] Alexander J. Blake,[1] Stephen T. Liddle[1]*

The terminal uranium nitride linkage is a fundamental target in the study of f-orbital participation in metal-ligand multiple bonding but has previously eluded characterization in an isolable molecule. Here, we report the preparation of the terminal uranium(V) nitride complex [UN(Tren^{TIPS})][Na(12-crown-4)$_2$] {in which Tren^{TIPS} = [N(CH$_2$CH$_2$NSiPr$^i_3$)$_3$]$^{3-}$ and Pr^i = CH(CH$_3$)$_2$} by reaction of the uranium(III) complex [U(Tren^{TIPS})] with sodium azide followed by abstraction and encapsulation of the sodium cation by the polydentate crown ether 12-crown-4. Single-crystal x-ray diffraction reveals a uranium-terminal nitride bond length of 1.825(15) angstroms (where 15 is the standard uncertainty). The structural assignment is supported by means of ^{15}N-isotopic labeling, electronic absorption spectroscopy, magnetometry, electronic structure calculations, elemental analyses, and liberation of ammonia after treatment with water.

Multiple bonding to uranium is exemplified by well-established U=O and U=NR double bonds in uranyl and imido complexes (*1*), respectively, and exploration of U=CR_2 double bonds in carbene derivatives now represents a burgeoning field (*2*–*4*). Nonetheless, prominent by their paucity are molecular U≡N triple bonds in uranium nitride complexes. A thorough understanding of the physicochemical properties of the uranium nitride linkage is key to predicting the long-term stability and reactivity of [UN]$_n$ as a ceramic nuclear fuel and to the ongoing debate regarding the nature and extent of uranium 5f and 6d valence orbital participation in uranium-ligand multiple bonding (*5*). Furthermore, understanding the inherent reactivity of the uranium nitride linkage with respect to electrophiles and nucleophiles is a prerequisite to identifying viable catalytic cycles (*6*). However, little is known about the intrinsic reactivity of the uranium nitride linkage because of the difficulties associated with synthesizing and solubilizing this functional group. Uranium nitrides

[1]School of Chemistry, University of Nottingham, University Park, Nottingham NG7 2RD, UK. [2]School of Chemistry and Photon Science Institute, University of Manchester, Oxford Road, Manchester M13 9PL, UK.

*To whom correspondence should be addressed. E-mail: stephen.liddle@nottingham.ac.uk

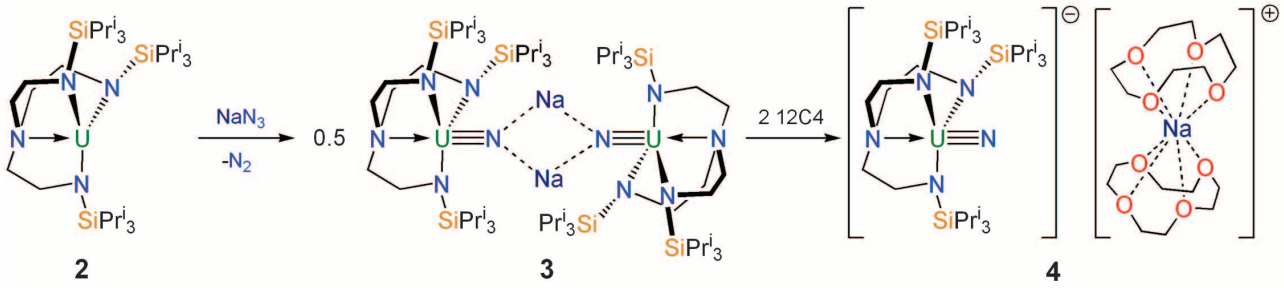

Scheme 1. Synthesis of compounds **3** and **4** from precursor **2**.

Exceptional Activity for Methane Combustion over Modular Pd@CeO Subunits on Functionalized AlO

M. Cargnello, J. J. Delgado Jaén, J. C. Hernández Garrido, K. Bakhmutsky, T. Montini, J. J. Calvino Gámez, R. J. Gorte, and P. Fornasiero

Science, 337 (6095),

Addressing a Burning Issue

Complete combustion of methane is required in order to avoid the unproductive emission of this greenhouse gas into the atmosphere. Palladium catalysts can help to promote complete combustion, but high-temperature operating conditions also promote aggregation of catalyst particles ("sintering") that lowers their surface area and overall activity. Cargnello *et al.* (p. 713; see the Perspective by Farrauto) report that cerium oxide–coated Pd catalyst particles could be fully dispersed on an alumina surface prepared with a hydrophobic coating. This treatment resisted Pd sintering up to temperatures of 800°C, and also enabled complete combustion of methane to occur at temperatures as low as 400°C.